

<https://doi.org/10.1038/s42004-025-01515-0>

Effect of additives on the high-temperature performance of a sodium bis(oxalato)borate in trimethyl phosphate electrolyte in sodium-ion batteries



Jonas Welch, Wessel W. A. van Ekeren, Jonas Mindemark & Reza Younesi

Sodium-ion batteries are a promising alternative to lithium-ion batteries due to their potential for lower cost and greater sustainability. However, achieving stable cycling performance, particularly at high mass-loadings and elevated temperatures, remains a challenge. The stable cycling of high mass-loading sodium-ion battery cells is here made possible by addition of prop-1-ene-1,3-sultone (PES) to a non-flammable and fluorine-free electrolyte solution of sodium bis(oxalato)borate (NaBOB) salt in triethyl phosphate (TEP). This study investigates the thermal stability and electrochemical performance of such electrolyte at 40 °C and 55 °C, contrasting their performance with base NaBOB in TEP with and without ethylene sulfate (DTD) additive and with a reference carbonate electrolyte of NaPF₆ in ethylene carbonate:diethylene carbonate (EC:DEC). Nuclear Magnetic Resonance spectroscopy was used to reveal degradation products formed in the electrolyte following a 4-weeks storage at 55 °C. Results from galvanostatic cycling at 55 °C demonstrated comparable performance of NaBOB–TEP + PES electrolyte and the reference carbonate electrolyte. The internal cell resistance was initially lower when cells were cycled at 55 °C than at 40 °C for all studied electrolytes.

To limit global warming, batteries are a key technology that can be used to greatly reduce greenhouse gas emissions from transportation and electricity storage^{1,2}. Lithium-ion batteries (LIB) are currently used in different applications as technology development and economies of scale have brought down the cost and increased energy density to attractive levels³. However, the rapidly growing adaption of LIB raises concerns regarding availability of raw materials used, such as lithium, cobalt, nickel, copper, and natural graphite³.

Sodium-ion batteries (SIB) are an alternative technology that share a number of qualities with LIB, but can be produced using fewer scarce resources and possibly lower cost^{4,5}. Also, the higher safety of SIB compared to LIB is among the described advantages⁶. As negative electrode in SIB, hard carbon is commonly used, combining a stable electrochemical cycling with low operating potential and reasonable intercalation capacity of sodium ions⁷. As positive electrode active material, a range of materials have been proposed, such as layered transition metal oxides⁸, polyanionic species⁹ and Prussian blue analogues¹⁰. Prussian white (Na_{2-x}Fe[Fe(CN)₆]_{1-y}·zH₂O) is a material with attractive properties, such as high theoretical sodium

storage capacity, relatively high electrode potential and naturally abundant precursor elements^{10,11}. It has also been shown to tolerate high temperature battery operation¹².

As in commercial LIBs, an electrolyte solution comprising sodium hexafluorophosphate (NaPF₆) electrolyte salt dissolved in at least two carbonate-based solvents is often used⁵. However, the toxicity and cost of NaPF₆ and the flammability of carbonate solvents motivates research into alternative electrolytes^{13,14}. Moreover, the low chemical stability of LiPF₆ and NaPF₆ at high storage or battery operation temperatures is also a known problem leading to reduced battery lifetime¹⁵⁻¹⁷.

Increasing the cycle life at elevated temperatures is an important, but often not prioritized, aspect of battery research and development^{18,19}. If batteries are more resilient to changes in temperature conditions, both in terms of safety and cycling performance, less complex and costly cooling and heating systems need to be integrated with battery cells in e.g., electric vehicles^{18,19}. This can also increase the practical energy density, as thermal management systems require a lot of space and weight. Electrolytes based on ionic liquids are sometimes proposed as thermally stable electrolytes, with

stability up to 300 °C and beyond²⁰. However, ionic liquids are expensive and rarely used in battery electrolytes for this reason. Zheng et al. studied degradation of LiPF₆ in EC:EMC (3:7, v/v) stored in different temperatures, and identified reaction products from degradation of PF₆⁻ initiated by traces of HF and water or short alcohols and proposed reaction mechanisms for their formation. To alleviate the thermal degradation, an alternative electrolyte solution based on lithium (fluorosulfonyl)(n-nonafluorobutanesulfonyl)imide (LiFNFSI) salt was proposed²¹. For SIB, Barnes et al. studied thermal degradation based on NaPF₆ in EC:EMC or EC:DMC in room temperature and 52 °C and with different moisture concentrations. There, degradation products of PF₆⁻ were also identified²².

Electrolyte additives have been extensively utilized to enhance the performance and cycle life of LIBs and SIBs^{23,24}. Among these additives, sulfur-containing compounds like prop-1-ene-1,3-sultone (PES) and 1,3,2-dioxathiolane 2,2-dioxide (DTD) or ethylene sulfate stand out for their ability to form protective layers on LIB anode surfaces²⁵. For instance, DTD has demonstrated the capability to improve coulombic efficiency, capacity retention, and low-temperature performance^{26,27}. Additionally, it suppresses graphite exfoliation in propylene carbonate (PC)-based electrolytes²⁶. However, while DTD effectively reduces gas release during high-temperature storage²⁵, this advantage does not extend to room temperature²³. Furthermore, SEI layers formed exclusively by DTD are insufficiently stable for prolonged cycling of NMC111-graphite cells at elevated temperatures (55 °C) when used with carbonate-based electrolytes²⁸. PES is another promising additive known for enhancing cycling performance in LIBs, with an optimal concentration of ~3 wt%²⁹. Compared to the widely used vinylene carbonate (VC) additive, PES significantly reduces gas formation at elevated temperatures³⁰. PES-containing electrolytes are capable of operating across a wide temperature range; however, cell resistance limits their performance at lower temperatures³¹. PES forms stable organic and inorganic sulfites in the SEI playing a key role in capacity retention²⁹ and enabling high-voltage cycling of NMC-graphite cells³¹. Additionally, PES prevents graphite exfoliation even under high-temperature conditions, such as 70 °C³¹.

While research into improving SIB systems is gaining momentum, studies on electrolyte additives for SIBs remain relatively limited. Most investigations focus on room-temperature performance and commonly used additives like fluoroethylene carbonate (FEC) and VC²⁴. Yan et al. combined the four electrolyte additives VC, succinonitrile (SN), 1,3-propane sultone (PS), and sodium difluoro(oxalate)borate (NaDFOB) to stabilize cycling at 55 °C of Na₃V₂(PO₄)₂F₃ (NVPF)—Hard carbon full cells³².

We have previously reported NaBOB salt dissolved in TEP solvent as a non-flammable, non-toxic electrolyte solution for SIBs^{33–35}. NaBOB has a limited solubility in common battery electrolyte solvents, and the concentration in TEP is limited to below 0.38 M. The performance of such an electrolyte in full-cell SIBs was further optimized by electrolyte additives. The results showed that PES and DTD were the most efficient additives in improving cycling performance, reaching a capacity retention of 80% after 450 cycles³⁶.

This study investigates electrolyte stability and cycling performance of full-cell SIBs at elevated temperatures of 40 °C and 55 °C using NaBOB-TEP electrolyte with the aforementioned additives. 1 M NaPF₆ in EC:DEC 1:1 v/v is here used as a standard reference electrolyte solution. Nuclear magnetic resonance (NMR) and visual inspection are used to investigate chemical changes in the electrolyte solutions upon storage at elevated temperatures. Electrochemical characterization including galvanostatic cycling and intermittent current interruption (ICI) technique are used to evaluate cell performance and internal resistance. Pressure analysis is used to investigate gas formation during formation cycling. The investigations show that the DTD additive is not thermally stable in the TEP-based electrolyte, as NMR analysis detects reaction products between DTD and TEP. In contrast, the PES additive enhances the cycling performance of the NaBOB-TEP electrolyte while also reducing total cell resistance and minimizing gas evolution during early cycling.

Results and discussion

Thermal stability of electrolyte solutions

To investigate thermal stability of the studied electrolytes, specific amounts of each electrolyte was subjected to 55 °C for one- and four-week time periods. As shown in Fig. 1, NaBOB-TEP electrolyte with DTD additive exhibited a color change to a weakly yellow/orange color progressively during storage. Conversely, no clear color changes were observed in any of the other electrolyte solutions.

The fresh and aged electrolytes stored for 1 and 4 weeks of storage at 55 °C were further analyzed using in ¹H, ¹³C, ¹⁹F and ³¹P NMR spectroscopy (Figs. S1–S13). ¹⁹F NMR spectra disclose that traces of breakdown products of PF₆⁻ form in the NaPF₆ in EC:DEC form after storage at 55 °C (Fig. 2a). Analogous to the interpretation made by Zheng et al., Barnes et al., Wilken et al., and Campion et al., the peaks appearing at around 80 and 82 ppm could correspond to difluorophosphoric acid (O=PF₂(OH) or PO₂F₂⁻)^{15,21,22,37}.

The NaBOB-TEP + DTD electrolyte, which was visibly discolored after storage on the hotplate and also to a smaller degree after storage at room temperature, fully lost its characteristic DTD peak in the ¹H spectrum (Fig. 2b) after storage at 55 °C for 4 weeks compared to four weeks at room temperature. This indicates that DTD decomposes at these conditions. The peaks detected at around 4.05 and 4.2 ppm are related to degradation products of DTD. Also, in the ¹³C spectrum (Fig. 2c), the DTD peak at 69.55 ppm diminishes and new peaks appeared at 70.97 (d), 69.46 (s), 68.82 (s), 63.90 (d) and 62.90 (d) and 61.65 (d) ppm (as can be more clearly seen in Fig. S7), indicating degradation of DTD at 55 °C. Some of these peaks are already visible in the sample from the electrolyte solution aged 4 weeks in room temperature, although in much smaller scale. This means that DTD

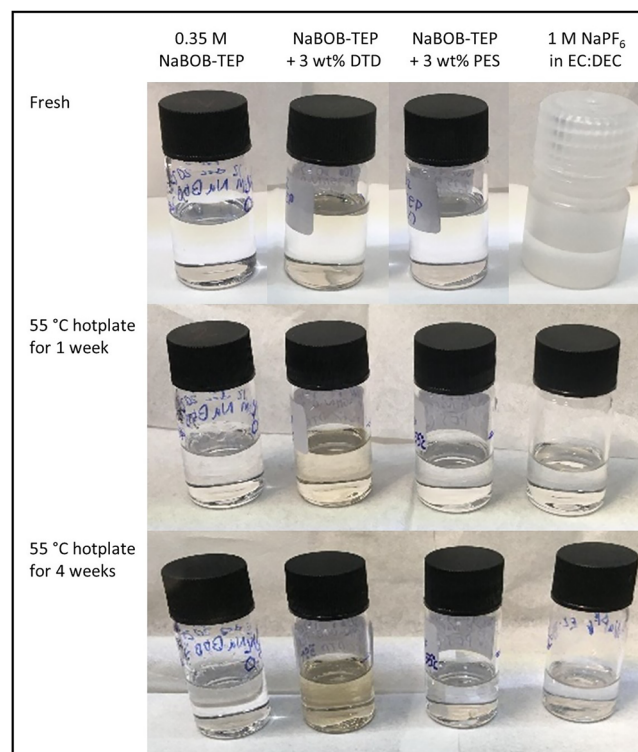


Fig. 1 | Visual color change after storage at elevated temperature. Digital photos of the freshly prepared electrolyte solutions and electrolyte solutions stored at 55 °C for 1 week or 4 weeks. After 1 week and 4 weeks small samples were taken from each vial for NMR spectroscopy analysis, which showed that the visible color change seen in the figure could be explained by a reaction between ethylene sulfate (DTD) and triethyl phosphate (TEP). Note that the sodium hexafluorophosphate (NaPF₆) in ethylene carbonate:diethylene carbonate (EC:DEC) electrolyte solution was stored in a polypropylene plastic vial during hot storage, it was only transferred to a glass vial for the photo.

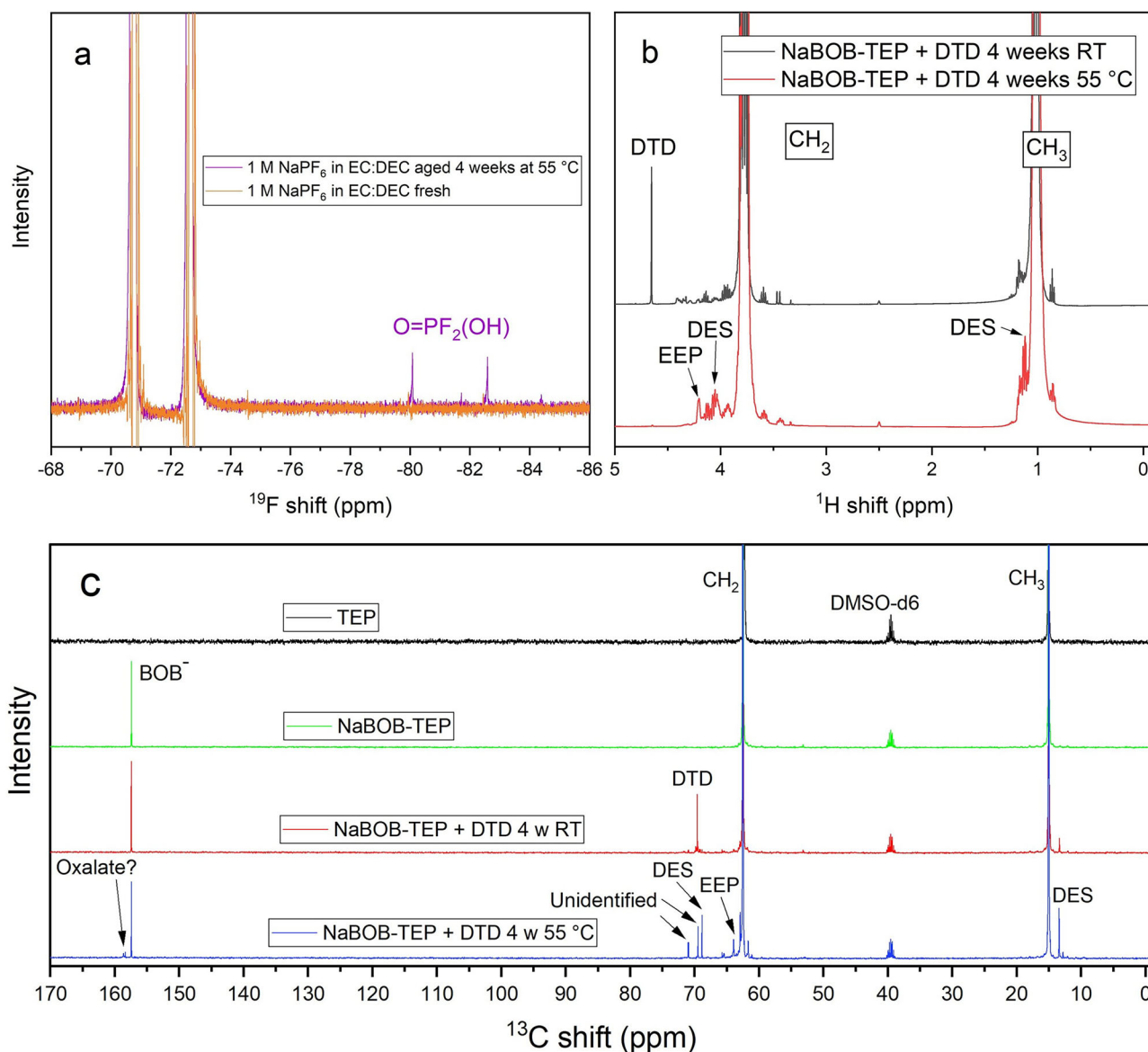


Fig. 2 | NMR spectra showing chemical degradation of two of the used electrolytes. a ^{19}F NMR before (orange) and after (purple) storage of 1 M NaPF_6 in EC:DEC for 4 weeks at 55 °C. Peaks at 80 and 82 ppm are identified as reaction products of PF_6^- , likely difluorophosphoric acid ($\text{O}=\text{PF}_2(\text{OH})$). **b** ^1H NMR spectra of 0.35 M NaBOB in TEP + 3 wt% DTD stored 4 weeks in room temperature (black, top) and

4 weeks at 55 °C (red, bottom). **c** ^{13}C NMR spectra of TEP (black), 0.35 M NaBOB in TEP (green), 0.35 M NaBOB in TEP + 3 wt% DTD stored for 4 weeks at room temperature (red), and 0.35 M NaBOB in TEP + 3 wt% DTD stored 4 weeks at 55 °C (blue), from top to bottom, respectively.

starts to degrade already at room temperature, which is consistent with the visible color change. The ^1H , ^{13}C , ^{19}F , and ^{31}P NMR spectra for NaBOB-TEP and NaBOB-TEP + PES electrolytes were remained unchanged (see Figs. S1–2, S5–6), and were thus chemically stable at 55 °C. The peaks detected around 3.45 ppm in the ^1H spectra and at 2.5 ppm in ^{31}P spectra for TEP-based electrolytes already before thermal storage (Figs. S1 – S3 and Figs. S10–12, respectively) are believed to come from solvent impurities.

To identify the degradation products in the NaBOB-TEP + DTD electrolyte, 2D NMR experiments were performed. First, a Heteronuclear Single Quantum Correlation (HSQC) NMR was made, but no peaks related to degradation products were detected (Fig. S14). Then, a Heteronuclear Multiple Bond Coherence (HMBC) NMR was made (Fig. 3), which shows correlations between ^1H and ^{13}C nuclei placed at least two atomic bonds apart in the molecule, as well as ^1H correlations with ^{13}C satellite peaks (one bond apart). Predicted ^1H and ^{13}C shifts in spectra from the Spectral Database for Organic Compounds and from a study by Xiao et al. were used

to correlate the HMBC peak positions labeled in Fig. 3 to bonding environments within the degradation product molecules^{38,39}. The suspected reaction products and the corresponding HMBC peak positions are further described in Table 1.

The degradation products, diethyl sulfate and 2-Ethoxy-1,3,2-dioxaphospholane 2-Oxide (ethyl ethylene phosphate), are hypothesized to be formed via a transesterification reaction, as depicted in Scheme 1, where the chemically different carbon atoms are also indicated.

Galvanostatic cycling performance

Figure 4 shows discharge capacities of full-cells galvanostatically cycled at elevated temperatures of 40 °C and 55 °C at a cycling rate of 0.2 C using different electrolytes studied in this work. The cells using 0.35 M NaBOB-TEP without any additives exhibited substantial capacity fading at both tested temperatures, although some improvement is observed compared to the previous cycling conducted at room temperature³⁶. This is

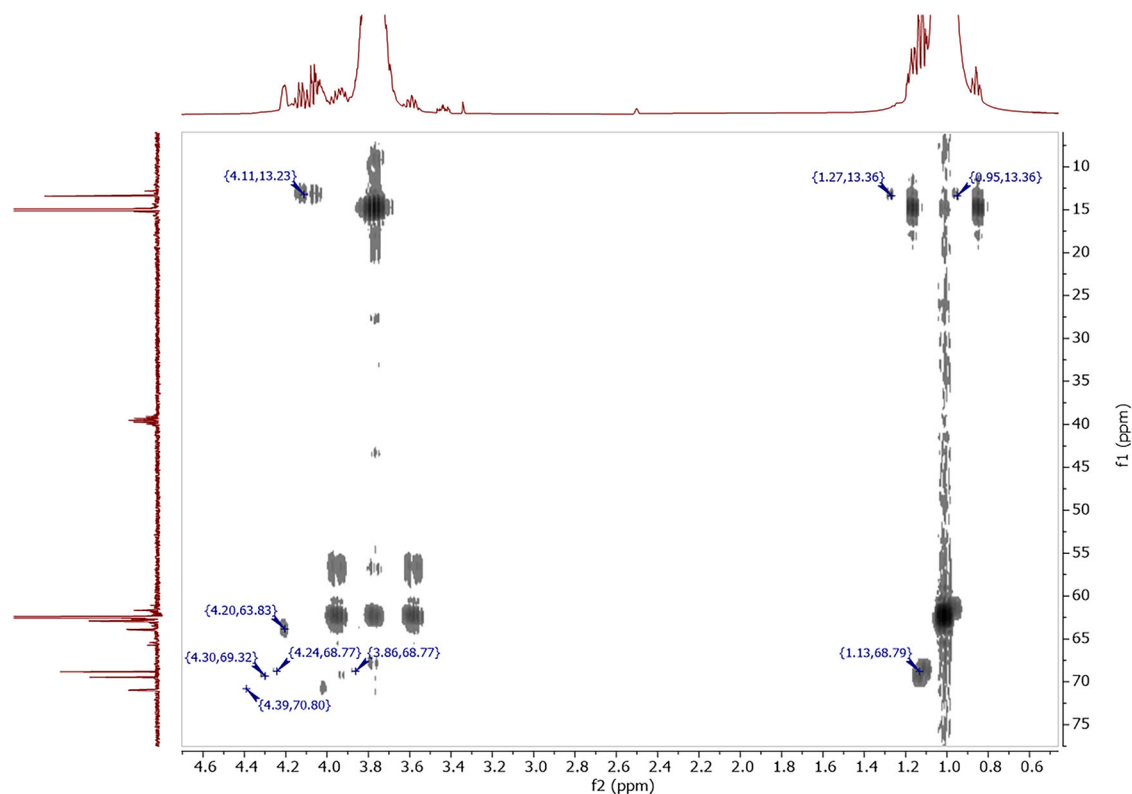


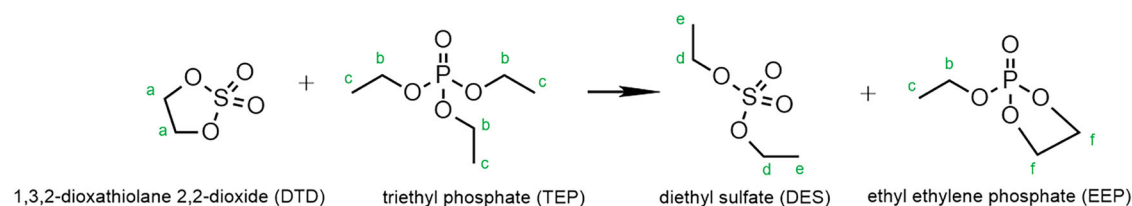
Fig. 3 | Evidence of reaction products of DTD and TEP. Heteronuclear Multiple Bond Coherence (HMBC) 2D NMR based on correlations between ¹H (horizontal) and ¹³C (vertical) nuclei in the NaBOB–TEP + DTD electrolyte. Some of the peaks

related to degradation products of DTD show HMBC correlation. Those are labeled in the figure and explained in Table 1.

Table 1 | Identified degradation products in the NaBOB–TEP + DTD electrolyte

¹ H peak	¹³ C peak	Compound	Correlating nuclei in HMBC
1.13	68.79	Diethyl sulfate	Proton on carbon <i>e</i> with carbon <i>d</i>
4.11	13.23	Diethyl sulfate	Proton on carbon <i>d</i> with carbon <i>e</i>
1.27, 0.95	13.36	Diethyl sulfate	Carbon <i>e</i> with proton on carbon <i>e</i> (¹³ C satellite peak)
4.24, 3.86	68.77	Diethyl sulfate	Carbon <i>d</i> with proton on carbon <i>d</i> (¹³ C satellite peak)
4.20	63.83	Ethyl ethylene phosphate	Proton on carbon <i>f</i> with other carbon <i>f</i>
4.30	69.32	Unidentified product 1	
4.39	70.80	Unidentified product 2	

Letters in green are referring to chemically different carbon atoms, indicated in Scheme 1.



Scheme 1 | Chemical reaction of DTD with TEP. Transesterification reaction degrading the NaBOB–TEP + DTD electrolyte solution. Chemically different carbon atoms have been marked with letters a–e in green.

consistent with our previous study, where 0.35 M NaBOB–TEP showed rapid fading in cells with high mass-loading electrodes (12 mg cm⁻²) unless a specific formation cycling protocol is applied⁴⁰. The addition of PES to NaBOB–TEP electrolyte led to large improvements in cycling stability as the cells cycled at both temperatures showed smaller fading, although the increased temperature predictably impacted capacity fading to some degree

(see Fig. 4c, d and S15). This increase in capacity fading can be partly alleviated by the use of a faster C-rate (see Fig. S15), which will decrease the time during which unwanted side-reactions can occur. The likely cause for the high thermal stability is that PES forms a sulfate-rich SEI which is effectively passivating the anode also at elevated temperature, preventing electrolyte degradation and gas formation⁴¹. The cells with the DTD additive

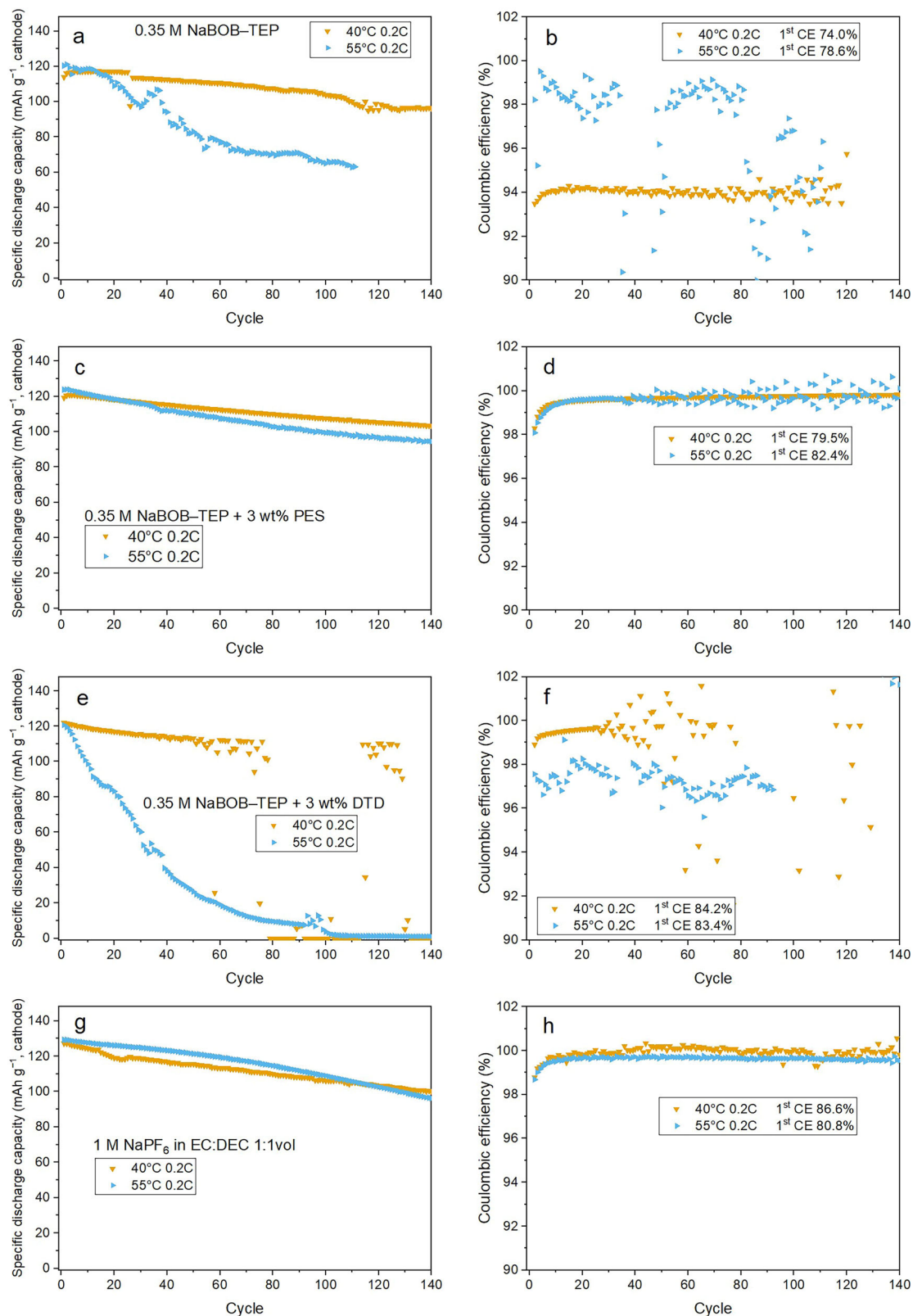


Fig. 4 | Capacity retention in galvanostatic cycling. Galvanostatic cycling of Prussian white – Hard carbon sodium-ion full cells at 40 °C (orange triangles) or 55 °C (blue triangles) in the left column and coulombic efficiency of the same cells in

the right column. Used electrolytes were in **a** and **b** 0.35 M NaBOB in TEP, in **c** and **d** 0.35 M NaBOB in TEP + 3 wt% PES, in **e** and **f** 0.35 M NaBOB in TEP + 3 wt% DTD and in **g** and **h** 1 M NaPF₆ in EC:DEC 1:1 by volume.

suffered from fast capacity degradation at 55 °C, whereas degradation was initially low at 40 °C after which cycling became unreliable (see Fig. 4e, f). This is likely related to the thermal instability of the DTD as discussed above, leading to a loss of DTD in the electrolyte and thus its ability to reform lost

SEI during cycling. Similarly, Madec et al. have shown that the use of DTD as a single additive in LIB cells using a LiPF₆ electrolyte produce an unstable SEI on graphite negative electrodes leading to accelerated capacity fading after 150 cycles²⁸.

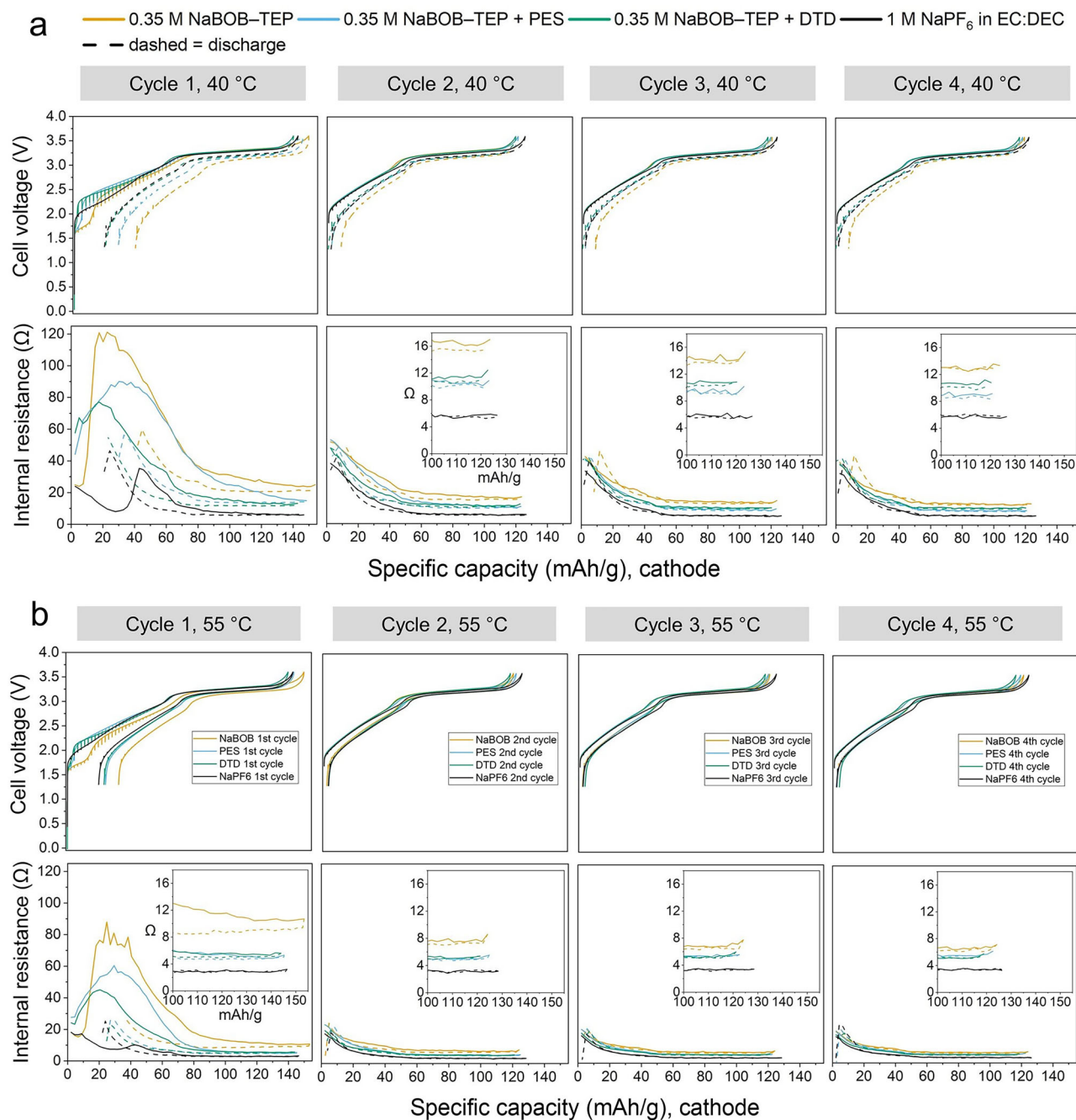


Fig. 5 | Voltage profiles and internal resistance in cells cycled at elevated temperature. Voltage profiles as well as internal cell resistance measured with the ICI method for Prussian white—Hard carbon full-cells with four different electrolytes

(0.35 M NaBOB-TEP (orange), 0.35 M NaBOB-TEP + 3 wt% PES (blue), 0.35 M NaBOB-TEP + 3 wt% DTD (green) and 1 M NaPF₆ in EC:DEC (black)), cycled at 0.2 C at **a** 40 °C and **b** 55 °C temperatures.

Figure 4g, h present the cycling results of the reference cells using the carbonate electrolyte. The cells exhibited a relatively higher first cycle CE, with the capacity fading of the cell cycled at 40 °C comparable to those with PES. However, the cell cycled at 55 °C showed an accelerated degradation after nearly 60 cycles. The addition of PES and DTD to the NaPF₆ in EC:DEC electrolyte showed detrimental effect on the long-term cycling performance of these cells with carbonate-based electrolytes, see Fig. S16, and are thus not suitable as high-temperature stable electrolytes.

Internal cell resistance

To investigate internal cell resistance during cycling, the ICI method was used (Fig. 5). During the initial stages of the first charge, the cells based on NaBOB-TEP with and without PES and DTD additives experienced high

resistance, attributed to SEI formation (Fig. 5a). Conversely, cells employing NaPF₆ in EC:DEC demonstrated comparatively lower resistance. Instead, the resistance slightly increases at around 40 mAh g⁻¹ during the first charge (Fig. 5a and S17). Throughout subsequent cycles, all the cells exhibited a consistent pattern during both charge and discharge, consistently peaking at low states of charge. This phenomenon may be linked to low Na⁺ mobility in the cathode active material when the Na content is high. It should be noted that among other parameters, the applied pressure to the pouch cells could have a large influence on the cell resistance. A higher controlled pressure may favor the cycling performance and lower the resistance in cells. To investigate the validity of the resistance calculations, a sample of resistance data points were scrutinized. Linear regression of the voltage as a function of the square root of time shows reasonably good fits, as can be seen in Fig. S18.

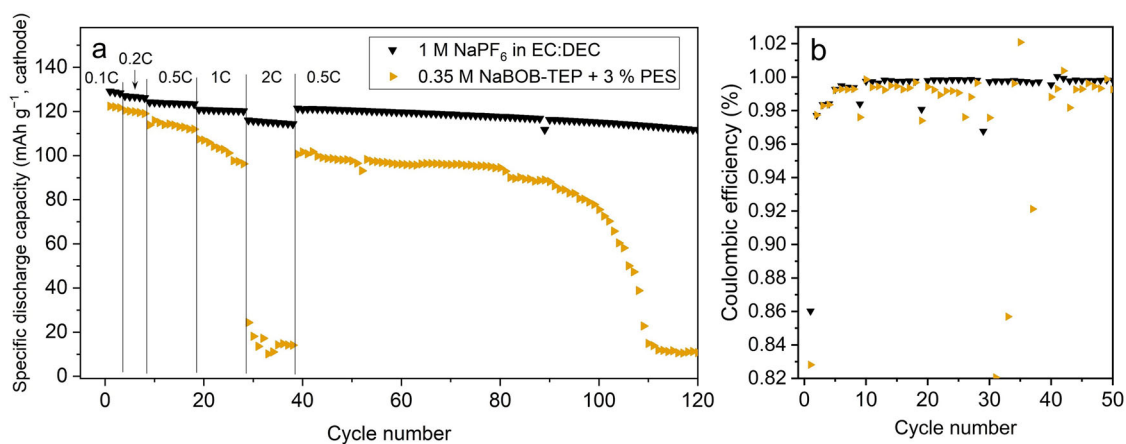


Fig. 6 | Galvanostatic cycling at increasing rate. Rate test at 55 °C for Prussian white – Hard carbon full cells using 0.35 M NaBOB–TEP + 3 wt% PES (orange triangles) and 1 M NaPF₆ in EC:DEC (black triangles) electrolytes, respectively. Specific capacity (a) and coulombic efficiency (b).

Rate capability

A rate-test was performed for the NaPF₆–EC:DEC and NaBOB–TEP + PES electrolytes at 55 °C, as the higher temperature enables higher ionic conductivity and potentially lower overall resistance. The results in Fig. 6 show that the cell with carbonate-based electrolyte outperformed the cell with 0.35 M NaBOB–TEP + PES at high C-rates as the latter suffered from major capacity fading at 2 C. The cause of this could be a result of the relatively lower ionic conductivity of NaBOB–TEP electrolyte, resulting in mostly active material close to the macro surface of the electrodes contributing with sodium ions. Alternatively, it could stem from a high-impedance SEI layer, as evidenced by the nearly doubled cell resistance measured via ICI (see Fig. 5).

Capacity retention after extended cycling pauses

To study the self-discharge, extended pause/relaxation test was carried out where cells were cycled at 0.2 C at 55 °C and were then stored at open circuit potential for 100 h after the 10th charge and the 20th discharge (Fig. 7a). The capacity values for the subsequent two discharges after the pause (Fig. 7b) was used to calculate the losses related to degradation taking place in the pause (total loss), losses that can be recouped in the second discharge after the pause (reversible loss) and the difference between the two (irreversible loss). The results overall (Fig. 7c) show that the losses for all three electrolytes are substantial, which is consistent with earlier studies on ageing of SIBs⁴². Furthermore, it is also evident that the losses are greater after a pause at charged state, of which the majority is recoverable (i.e., reversible losses) for NaPF₆ in EC:DEC electrolyte and NaBOB–TEP without additive, whereas for the NaBOB–TEP with PES additive, the irreversible losses dominated. The reversible losses during the pause may be attributed to a redox shuttling mechanism, where guest molecules present in the electrolyte carry charge by diffusion between the anode and cathode while repeatedly undergoing reduction and oxidation. Sloop et al. linked this phenomenon to the shuttling of CO₂ formed by reduction of EC⁴¹. Melin et al. has showed that CO₂ is also produced from the reduction of LiBOB, and thus could also potentially contributing to the effect⁴³. The irreversible losses are likely caused by SEI dissolution and subsequent re-formation, which consumes part of the sodium inventory. In the case of PES-containing electrolyte, this effect may be exacerbated by a more organic SEI that is more prone to dissolution^{31,44} compared to the more inorganic SEI formed by NaBOB and TEP³⁶. A pause at the discharged state did not result in reversible losses, and irreversible losses were slightly lower compared to those at the charged state for all three electrolytes. The voltage curves seen in Fig. 7a show that NaBOB–TEP electrolyte without additive follow a self-discharge curve similar to that of NaPF₆–EC:DEC but with a faster overall self-discharge, which is also evident in the lower discharge capacity directly following the pause. On the other hand, the cell with the electrolyte with PES additive experience a faster

drop below 3.45 V than the two other electrolytes, but then stabilizes and show a much lower decrease in voltage, ending the pause at a higher value of 3.34 V compared to 3.27 V for NaPF₆ in EC:DEC and 3.23 V (corresponding to the higher plateau of Prussian white) for NaBOB–TEP without additive. This phenomenon is also evident in the much lower reversible losses for the electrolyte with PES additive (Fig. 7c). From a user perspective, a cell with low self-discharge is useful, since you have more useful capacity after a pause, however from a state of health perspective, the irreversible losses need to be considered. In that regard, the losses are comparable between the studied electrolytes, and only marginally higher for the NaBOB–TEP electrolyte with PES additive.

Gas pressure evolution in early cycling

The pressure buildup in cells during initial three cycles at 55 °C was measured, as shown in Fig. 8. The cells with NaBOB in TEP or with NaPF₆ in EC:DEC electrolytes showed a substantial increase in the cell pressure, i.e. 20 mbar and 25 mbar respectively (Fig. 8a, c). However, the pressure increase in the cell using NaBOB–TEP + PES electrolyte is considerably lower (i.e. around 10 mbar), indicating that the surface of the negative electrode is effectively passivated using PES additive (Fig. 8b). It should be noted that these cells experience a leakage specified to maximum 0.3 mbar h⁻¹ by the supplier, and thus the figures below have been corrected for this leakage by an addition of a linear component to the data corresponding to the slope of the measured pressure during the 2 h directly before the initiation of the galvanostatic cycling. The original pressure data is available in Fig. S19. These results are consistent with literature for LIB cells, where Xia et al. showed that PES considerably lowers gas volume formed in Li(Ni_{1/3}Mn_{1/3}Co_{1/3})O₂/graphite pouch cells using a standard LiPF₆ electrolyte upon cycling at 40 °C and storage at 60 °C, compared to the VC additive or no additive³⁰.

Conclusions

The thermal stability of NaBOB–TEP electrolytes with PES or DTD additives as well as a reference carbonate electrolyte based on NaPF₆ in EC:DEC was studied through storage at elevated temperature of 55 °C. NMR spectroscopy results revealed partial degradation of NaPF₆ likely forming difluorophosphoric acid (O=PF₂(OH)), and full degradation of DTD in a transesterification reaction with TEP solvent forming diethyl sulfate and ethyl ethylene phosphate. The degradation of DTD in the NaBOB–TEP electrolyte solution starts already at room temperature, discoloring the electrolyte. However, NaBOB–TEP electrolyte with and without PES additive remained stable after 4 weeks storage at 55 °C.

The electrochemical performance of Prussian white–hard carbon full-cells was investigated at 40 °C and 55 °C under different cycling protocols, including galvanostatic cycling with and without extended relaxation time

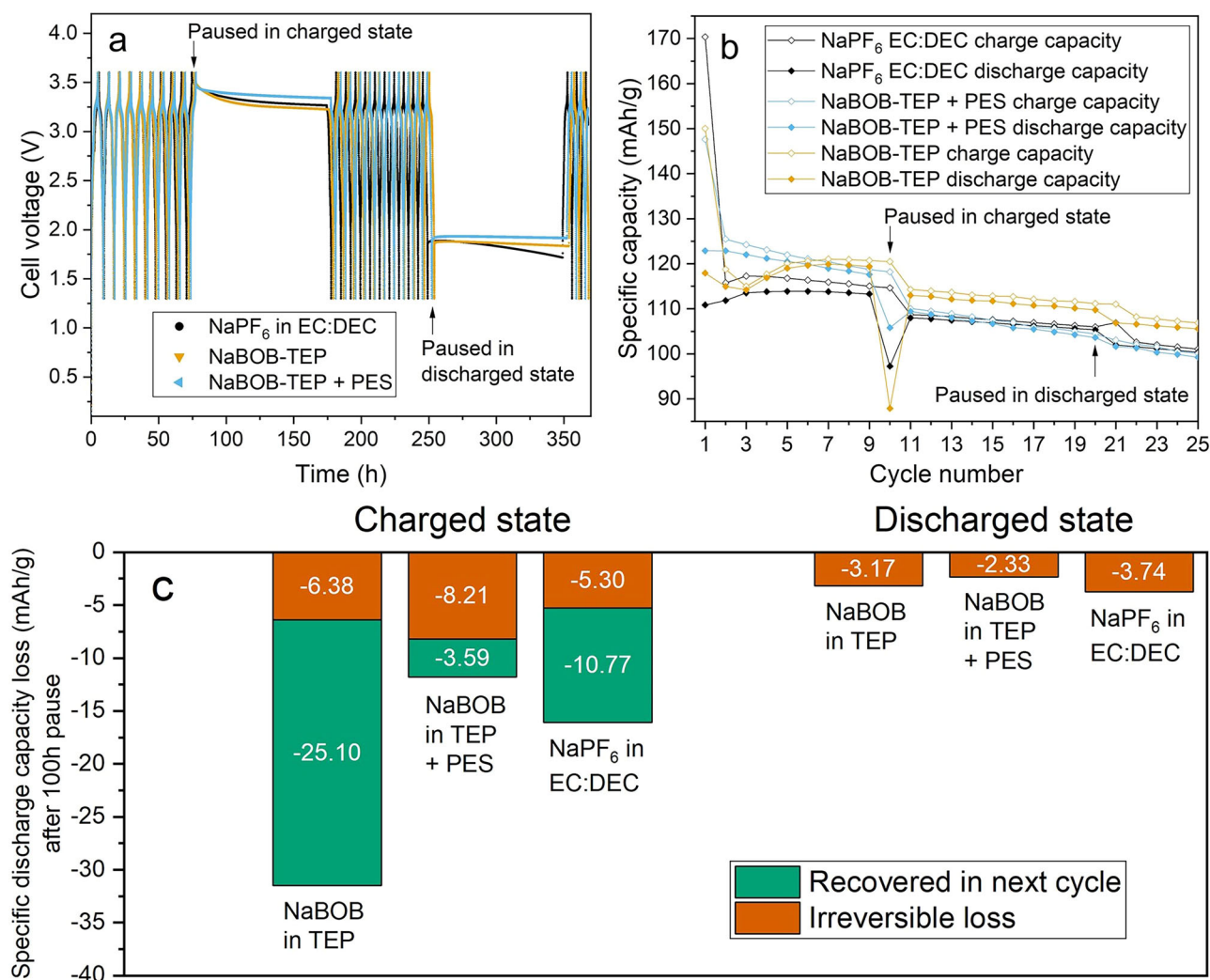


Fig. 7 | Capacity loss after extended cycling pauses. Galvanostatic cycling combined with extended relaxation test of Prussian white—Hard carbon full-cells using the three electrolytes of 0.35 M NaBOB in TEP (orange triangles or diamonds), 0.35 M NaBOB in TEP + 3 wt% PES (blue triangles or diamonds) or 1 M NaPF₆ in EC:DEC 1:1 (black circles or diamonds). **a** Overview of the voltage profiles. The cells were cycled at 55 °C using 0.2 C rate, and relaxed for 100 h after charge number 10 and relaxed for 100 h after discharge number 20. **b** Corresponding charge and

discharge capacities for the same cells. Open diamonds for charge capacities and filled diamonds for discharge capacities. **c** Calculated losses in the first discharge following the pause compared to the last discharge before the pause, for pauses at charged and discharged states, respectively. Irreversible loss (red) remains also in the second discharge after the pause whereas the capacity which is recovered in the next cycle (green) is the reversible loss that is only seen in the first discharge after the pause.

and different cycling rates. 0.35 M NaBOB in TEP with 3 wt% PES electrolyte solution showed promising results, obtaining stable cycling at 55 °C at 0.2 C rate and reaching comparable capacity retention after 140 cycles as 1 M NaPF₆ in EC:DEC at the same condition. The NaPF₆ electrolyte on the other hand experienced an acceleration in capacity fade after around 100 cycles. Rate capability tests at 55 °C exhibited inferior performance for NaBOB-TEP + PES electrolyte compared to NaPF₆ in EC:DEC, which could be mainly due to the relatively lower ionic conductivity of this electrolyte and/or higher SEI-layer impedance, as is implied by the higher cell resistance.

PES additives decreased the amount of gas formed during the initial cycles and thus the cell pressure was lower in the cell with NaBOB-TEP + PES electrolyte compared to the cells with NaBOB-TEP or NaPF₆ in EC:DEC. The cell resistance formed during the 1st charge was higher in the cells with NaBOB in TEP with and without additives, compared to the reference cell with NaPF₆ in EC:DEC. However, that decreased to smaller values similar to the resistance in NaPF₆ in EC:DEC cells from the 1st discharge, and remained more or less the same in the following cycles. All this together suggest that the ratio of solid to gas species formed during the

1st cell charge is higher in NaBOB-TEP + PES electrolyte compared to that in NaBOB-TEP or NaPF₆ in EC:DEC.

Furthermore, pause tests show a lower self-discharge rate of cells with NaBOB-TEP + PES electrolyte compared to NaPF₆ EC:DEC, which is evident by the slower voltage decay and lower reversible capacity loss when paused in the charged state. However, the irreversible loss is somewhat higher than for the reference carbonate electrolyte.

Overall, NaBOB-TEP + 3 wt% PES as a non-flammable and fluorine-free electrolyte is a promising alternative to flammable carbonate-based electrolytes, with potential use in commercial SIB suitable for applications with higher operating temperatures.

Methods

Materials, electrolyte preparation and thermal stability test

Electrolytes were prepared from NaBOB synthesized and purified, according to the method described earlier³⁸. NaPF₆ (Stella[®], 99%) was dried at 120 °C in a vacuum oven before use. PES (TCI chemicals[®], ≥99%) and DTD (TCI chemicals[®], ≥98%) were used as electrolyte additives. TEP (Sigma-Aldrich[®], ≥99.8%) as well as EC:DEC 1:1 (Gotion[®]) was kept over

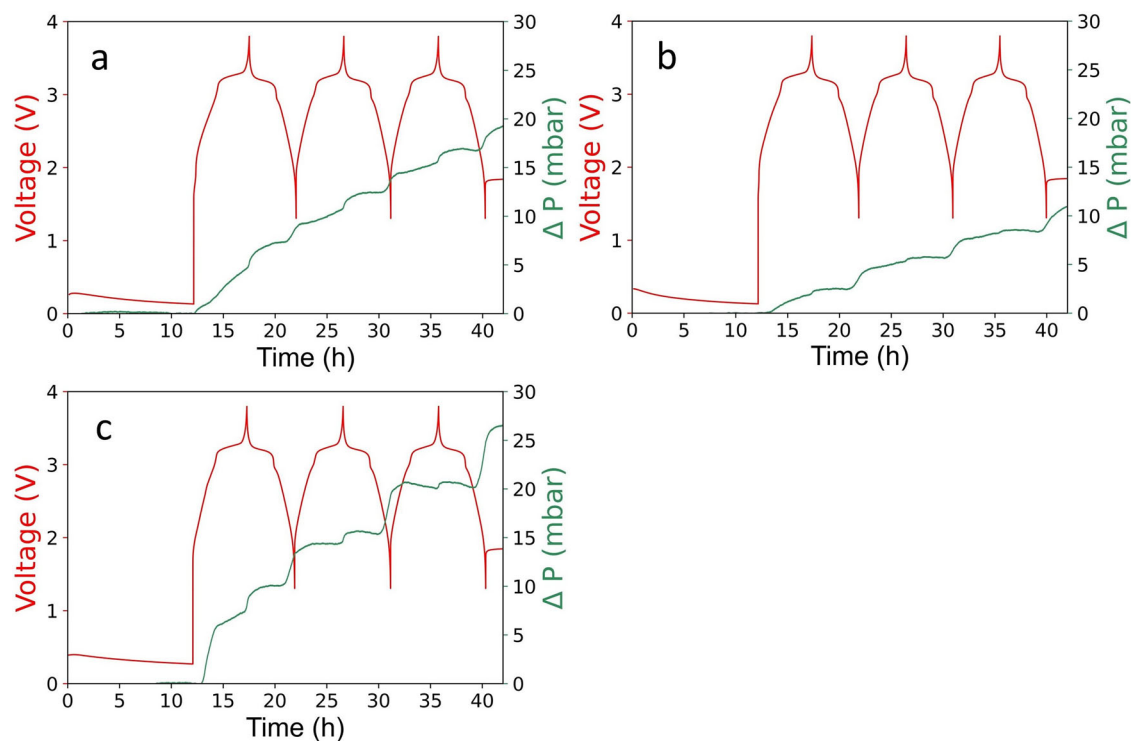


Fig. 8 | Pressure evolution in first cycles. Pressure analysis (green lines, right-hand scale) of full-cells cycled at 55 °C at 0.2 C rate using **a** 0.35 M NaBOB in TEP, **b** 0.35 M NaBOB in TEP + 3 wt% PES and **c** 1 M NaPF₆ in EC:DEC electrolyte solutions, as well as voltage profiles for the same cells (red lines, left-hand scale). Note

that there is a natural leakage of the pressure cells specified to maximum 0.3 mbar h⁻¹ by the supplier, and that the relative pressures have been corrected to reflect an estimate of the pressure evolved from the cell components during the galvanostatic cycling. The original pressure data is available in Fig. S19.

molecular sieves at least 1 day before electrolyte preparation. NaBOB–TEP electrolyte solutions for electrochemical experiments were prepared volumetrically in glass vials, whereas the NaPF₆ in EC:DEC electrolyte solutions were prepared and stored in aluminum vials. All electrolytes were prepared and stored in an argon-filled glovebox with water and moisture levels below 1 ppm. Moisture content in electrolyte solutions was 14.5 ppm for NaPF₆ in EC:DEC and <34 ppm for NaBOB in TEP, measured with Karl Fisher titration.

Other separate batches of electrolyte solutions, specifically prepared for the storage test at elevated temperature, were treated as follows. NaBOB–TEP, NaBOB–TEP + PES and NaBOB–TEP + DTD electrolyte solutions were all prepared and stored in glass vials. NaPF₆ in EC:DEC was prepared in a glass vial, poured to an aluminum vial and stored for 20 days in room temperature, and then poured to a polypropylene plastic vial before elevated temperature storage. The four vials with the mentioned solutions were stored at 55 °C for 4 weeks to investigate changes in color and chemical contents. All four vials were placed in a tailor-made aluminum block placed on a temperature-controlled hotplate, with the thermocouple for the hotplate fitted in a hole in the block. Before and after 1 and 4 weeks of storage, electrolytes were photographed with a mobile phone camera to visualize color changes as well as characterized with ¹H, ¹³C, ¹⁹F, and ³¹P NMR.

NMR characterizations

Four hundred megahertz NMR was made using a JEOL RESONANCE ECZ400S spectrometer. 540 microlitres of the studied electrolyte solution were placed in an NMR glass tube in the argon-filled glovebox. Deuterated dimethyl sulfoxide (DMSO-d₆) was placed in coaxial insert which were in turn placed in the NMR tube, which was then sealed with a lid and parafilm. NMR samples were measured within 2 days after being taken out of the glovebox. ¹H spectra were referenced to DMSO-d₅ traces at 2.500 ppm and ¹³C spectra were referenced to DMSO-d₆ at 39.52 ppm⁴⁵, whereas ¹⁹F spectra were referenced relative to the peak of NaPF₆ at -72.7 ppm, as was done by Barnes et al.²². Spectra were normalized to the height of the largest peak.

Battery cell assembly

Electrodes were provided by LiFeSiZE AB[®], using commercial Prussian white powder Fennac produced by Altris AB[®] (12 mg cm⁻²) and hard carbon (7 mg cm⁻²), with an N/P ratio of 1.1 for the full cells. More specific details regarding composition etc. are found in the earlier publication³⁶. Electrode disks were cut from foil sheets to 20 mm in diameter, before dried for 15 h in a vacuum oven at 170 °C, after which they were kept in an argon-filled glovebox. Pouch cells were assembled in the glovebox with 150 μL electrolyte, Dreamweaver gold separator, and 5 mm wide current collector tabs cut from thicker Al foil and placed behind each electrode disc.

Galvanostatic cycling and Intermittent current interruption (ICI)

Full cells were cycled at 40 °C or 55 °C in a Novonix High Precision Charger System or Arbin Instruments battery testing system. The internal resistance of some cells was studied with ICI, for which an Arbin Instruments battery testing system was used. Some of the cells were equipped with reference electrodes based on preconditioned Prussian white, as in the previous publication³⁶. Every 5 min, a 1 s pause with a recorded datapoint every 0.1 s was initiated. As the pause is initiated, there is a voltage drop linearly proportional to $t^{1/2}$. The instantaneous voltage drop at $t = 0$ was extrapolated from the 10 data points within the pause, and using Ohm's law, resistance was calculated for each pause⁴⁶. The calculated resistance values were then averaged for each cycle.

For the cycling rate tests, discharge rate was increased from 0.2 C to 0.5 C, 1 C, 2 C, 4 C and 8 C with 10 cycles on each rate, whereas charge rate was kept at 0.2 C. The extended relaxation tests were carried out by adding 100 h pause after the 10th charge and 20th discharge, to investigate capacity loss at charged and discharged states, respectively.

Pressure analysis

Pressure was measured during the three first 0.2 C galvanostatic cycles for the full cells assembled in PAT-Cell-Press from EL-cell[®] according to the method described in the earlier publication³⁶. Tests were performed at 55 °C

for the 0.35 M NaBOB–TEP, 0.35 M NaBOB–TEP + 3 wt% PES, and 1 M NaPF₆ in EC:DEC electrolytes.

Data availability

All relevant data are available from the authors upon request. Reza Younesi will be responsible for replying to this request. Galvanostatic cycle data is either in .csv (Novonix) or .xlsx file format (Arbin). NMR data is in the .jdf file format. This galvanostatic and NMR data is further summarized in Origin in .opju file format. Pressure analysis data is also in the .xlsx file format.

Received: 11 September 2024; Accepted: 4 April 2025;

Published online: 26 April 2025

References

- Jacobson, M. Z. Review of solutions to global warming, air pollution, and energy security. *Energy Environ. Sci.* **2**, 148–173 (2009).
- Jacobson, M. Z. Batteries or hydrogen or both for grid electricity storage upon full electrification of 145 countries with wind-water-solar? *iScience*, **27**, <https://doi.org/10.1016/j.isci.2024.108988> (2024).
- Orangi, S. et al. Trajectories for lithium-ion battery cost production: can metal prices hamper the deployment of lithium-ion batteries? *Batter. Supercaps* **6**, <https://doi.org/10.1002/batt.202300346> (2023).
- Vaalma, C., Buchholz, D., Weil, M. & Passerini, S. A cost and resource analysis of sodium-ion batteries. *Nat. Rev. Mater.* **3**, 18013 (2018).
- Hwang, J.-Y., Myung, S.-T. & Sun, Y.-K. Sodium-ion batteries: present and future. *Chem. Soc. Rev.* **46**, 3529–3614 (2017).
- Rudola, A., Wright, C. J. & Barker, J. Reviewing the safe shipping of lithium-ion and sodium-ion cells: a materials chemistry perspective. *Energy Mater. Adv.* **2021**, <https://doi.org/10.34133/2021/9798460> (2021).
- Fitzpatrick, J. R., Costa, S. I. R. & Tapia-Ruiz, N. Sodium-ion batteries: current understanding of the sodium storage mechanism in hard carbons. *Johns. Matthey Technol. Rev.* **66**, 44–60 (2022).
- Yabuuchi, N. et al. P2-type Na_x[Fe_{1/2}Mn_{1/2}]O₂ made from earth-abundant elements for rechargeable Na batteries. *Nat. Mater.* **11**, 512–517 (2012).
- Gover, R. K. B., Bryan, A., Burns, P. & Barker, J. The electrochemical insertion properties of sodium vanadium fluorophosphate, Na₃V₂(PO₄)₂F₃. *Solid State Ion.* **177**, 1495–1500 (2006).
- Wang, L. et al. Rhombohedral prussian white as cathode for rechargeable sodium-ion batteries. *J. Am. Chem. Soc.* **137**, 2548–2554 (2015).
- Brant, W. R. et al. Selective control of composition in prussian white for enhanced material properties. *Chem. Mater.* **31**, 7203–7211 (2019).
- Sun, R. & You, Y. Prussian white cathode materials for all-temperature sodium-ion batteries. *ACS Appl. Mater. Inter.* **15**, 44599–44606 (2023).
- Gond, R., van Ekeren, W., Mogensen, R., Naylor, A. J. & Younesi, R. Non-flammable liquid electrolytes for safe batteries. *Mater. Horiz.* **8**, 2913–2928 (2021).
- Mogensen, R., Colbin, S. & Younesi, R. An attempt to formulate non-carbonate electrolytes for sodium-ion batteries. *Batter. Supercaps* **4**, 791–814 (2021).
- Campion, C. L., Li, W. & Lucht, B. L. Thermal decomposition of LiPF₆-based electrolytes for lithium-ion batteries. *J. Electrochem. Soc.* **152**, A2327 (2005).
- Lee, H. H., Wan, C. C. & Wang, Y. Y. Thermal stability of the solid electrolyte interface on carbon electrodes of lithium batteries. *J. Electrochem. Soc.* **151**, A542 (2004).
- Sloop, S. E., Pugh, J. K., Wang, S., Kerr, J. B. & Kinoshita, K. Chemical reactivity of PF₅ and LiPF₆ in ethylene carbonate/dimethyl carbonate solutions. *Electrochem. Solid State Lett.* **4**, A42 (2001).
- Lin, X., Salari, M., Arava, L. M. R., Ajayan, P. M. & Grinstaff, M. W. High temperature electrical energy storage: advances, challenges, and frontiers. *Chem. Soc. Rev.* **45**, 5848–5887 (2016).
- Rao, Z. & Wang, S. A review of power battery thermal energy management. *Renew. Sustain. Energy Rev.* **15**, 4554–4571 (2011).
- Chagas, L. G., Jeong, S., Hasa, I. & Passerini, S. Ionic liquid-based electrolytes for sodium-ion batteries: tuning properties to enhance the electrochemical performance of manganese-based layered oxide cathode. *ACS Appl. Mater. Inter.* **11**, 22278–22289 (2019).
- Zheng, L. et al. Li[(FSO₂)_n(C₄F₉SO₂)_N] versus LiPF₆ for graphite/LiCoO₂ lithium-ion cells at both room and elevated temperatures: A comprehensive understanding with chemical, electrochemical and XPS analysis. *Electrochim. Acta* **196**, 169–188 (2016).
- Barnes, P. et al. A non-aqueous sodium hexafluorophosphate-based electrolyte degradation study: formation and mitigation of hydrofluoric acid. *J. Power Sources* **447**, 227363 (2020).
- Wang, D. Y. et al. A systematic study of electrolyte additives in Li[Ni_{1/3}Mn_{1/3}Co_{1/3}]O₂ (NMC)/graphite pouch cells. *J. Electrochem. Soc.* **161**, A1818 (2014).
- Huang, Z.-X. et al. Electrode/electrolyte additives for practical sodium-ion batteries: a mini review. *Inorg. Chem. Front.* **10**, 37–48 (2023).
- Tong, B. et al. Sulfur-containing compounds as electrolyte additives for lithium-ion batteries. *Infomat* **3**, 1364–1392 (2021).
- Sano, A. & Maruyama, S. Decreasing the initial irreversible capacity loss by addition of cyclic sulfate as electrolyte additives. *J. Power Sources* **192**, 714–718 (2009).
- Wu, Z. et al. The roles of sulfur-containing additives and their working mechanism on the temperature-dependent performances of Li-ion batteries. *J. Electrochem. Soc.* **165**, A2792 (2018).
- Madec, L. et al. Effect of sulfate electrolyte additives on LiNi_{1/3}Mn_{1/3}Co_{1/3}O₂/graphite pouch cell lifetime: correlation between XPS surface studies and electrochemical test results. *J. Phys. Chem. C.* **118**, 29608–29622 (2014).
- Li, B. et al. Properties of solid electrolyte interphase formed by prop-1-ene-1,3-sultone on graphite anode of Li-ion batteries. *Electrochim. Acta* **105**, 1–6, <https://doi.org/10.1016/j.electacta.2013.04.142> (2013).
- Xia, J. et al. Comparative study on Prop-1-ene-1,3-sultone and vinylene carbonate as electrolyte additives for Li(Ni_{1/3}Mn_{1/3}Co_{1/3})O₂/graphite pouch cells. *J. Electrochem. Soc.* **161**, A1634 (2014).
- Song, W. et al. Effect of prop-1-ene-1,3-sultone on the performances of lithium cobalt oxide/graphite battery operating over a wide temperature range. *Int. J. Electrochem. Sci.* **12**, 10749–10762 (2017).
- Yan, G. et al. A new electrolyte formulation for securing high temperature cycling and storage performances of Na-ion batteries. *Adv. Energy Mater.* **9**, 1901431 (2019).
- Mogensen, R., Colbin, S., Menon, A. S., Bjorklund, E. & Younesi, R. Sodium Bis(oxalato)borate in trimethyl phosphate: a fire-extinguishing, fluorine-free, and low-cost electrolyte for full-cell sodium-ion batteries. *ACS Appl. Energy Mater.* **3**, 4974–4982 (2020).
- Mogensen, R., Buckel, A., Colbin, S. & Younesi, R. A wide-temperature-range, low-cost, fluorine-free battery electrolyte based on sodium bis(oxalato)borate. *Chem. Mater.* **33**, 1130–1139 (2021).
- Colbin, L. O. S. et al. A halogen-free and flame-retardant sodium electrolyte compatible with hard carbon anodes. *Adv. Mater. Interfaces* **8**, <https://doi.org/10.1002/admi.202101135> (2021).
- Welch, J. et al. Optimization of sodium bis(oxalato)borate (nabob) in triethyl phosphate (TEP) by electrolyte additives. *J. Electrochem. Soc.* **169**, <https://doi.org/10.1149/1945-7111/aca55e> (2022).
- Wilken, S., Treskow, M., Scheers, J., Johansson, P. & Jacobsson, P. Initial stages of thermal decomposition of LiPF₆-based lithium ion battery electrolytes by detailed Raman and NMR spectroscopy. *RSC Adv.* **3**, 16359–16364 (2013).

38. Spectral Database for Organic Compounds (SDBS); ^1H and ^{13}C NMR spectra; SDBS No.: 310; CAS 64-67-5; <https://sdb.sdb.aist.go.jp> (accessed March 13, 2024).
39. Xiao, C., Wang, Y.-C., Du, J., Chen, X.-S. & Wang, J. Kinetics and mechanism of 2-Ethoxy-2-oxo-1,3,2-dioxaphospholane Polymerization initiated by stannous octoate. *Macromolecules* **39**, <https://doi.org/10.1021/ma0615396> (2006).
40. Buckel, A. et al. Importance of first cycle conditions on the electrochemical performance of hard carbon and prussian white based sodium-ion batteries using fire resistant, fluorine-free electrolyte. *Batter. Supercaps* **7**, <https://doi.org/10.1002/batt.202300533> (2024).
41. Sloop, S. E., Kerr, J. B. & Kinoshita, K. The role of Li-ion battery electrolyte reactivity in performance decline and self-discharge. *J. Power Sources* **119-121**, 330–337 (2003).
42. Ma, L. A. et al. Fundamental understanding and quantification of capacity losses involving the negative electrode in sodium-ion batteries. *Adv. Sci.* **11**, 2306771 (2024).
43. Melin, T., Lundström, R. & Berg, E. J. Elucidating the reduction mechanism of lithium bis(oxalato)borate. *J. Phys. Chem. Lett.* **15**, 2537–2541 (2024).
44. Self, J., Hall, D. S., Madec, L. & Dahn, J. R. The role of prop-1-ene-1,3-sultone as an additive in lithium-ion cells. *J. Power Sources* **298**, 369–378 (2015).
45. Babij, N. R. et al. NMR chemical shifts of trace impurities: industrially preferred solvents used in process and green chemistry. *Org. Process Res. Dev.* **20**, 661–667 (2016).
46. Lacey, M. J. Influence of the electrolyte on the internal resistance of lithium–sulfur batteries studied with an intermittent current interruption method. *ChemElectroChem* **4**, 1997–2004 (2017).
- pressure analysis and plotted the data from it. W.W.A.v.E. also assisted in the NMR experiments. J.M. assisted in the NMR experiment planning and interpretation of the NMR results. J.W. wrote the manuscript and R.Y. assisted.

Funding

Open access funding provided by Uppsala University.

Competing interests

The authors declare no competing interests.

Additional information

Supplementary information The online version contains supplementary material available at <https://doi.org/10.1038/s42004-025-01515-0>.

Correspondence and requests for materials should be addressed to Reza Younesi.

Peer review information *Communications Chemistry* thanks the anonymous reviewers for their contribution to the peer review of this work.

Reprints and permissions information is available at <http://www.nature.com/reprints>

Publisher's note Springer Nature remains neutral with regard to jurisdictional claims in published maps and institutional affiliations.

Open Access This article is licensed under a Creative Commons Attribution 4.0 International License, which permits use, sharing, adaptation, distribution and reproduction in any medium or format, as long as you give appropriate credit to the original author(s) and the source, provide a link to the Creative Commons licence, and indicate if changes were made. The images or other third party material in this article are included in the article's Creative Commons licence, unless indicated otherwise in a credit line to the material. If material is not included in the article's Creative Commons licence and your intended use is not permitted by statutory regulation or exceeds the permitted use, you will need to obtain permission directly from the copyright holder. To view a copy of this licence, visit <http://creativecommons.org/licenses/by/4.0/>.

© The Author(s) 2025

Acknowledgements

The authors would like to acknowledge Christopher Folkesson Welch for his contribution to the interpretation of the NMR spectra, and the financial contributions from the Swedish Energy Agency via project no. 50177–1 and via StandUp for Energy, from VINNOVA via BASE (Batteries Sweden, no. 2019–00064), and from the SuSaNa project under M-ERA-Net call 2021 (G.A. no 958174) via funding from VINNOVA (projects no. 2022-01465).

Author contributions

J.W. and R.Y. co-planned the project. J.W. Performed all experiments and characterizations except pressure analysis. W.W.A.v.E. performed the